



A molecular dynamics study on the thermal properties of carbon-based gold nanoparticles

E. Gowdini¹ · A. A. Ahmad² · A. Mabudi³ · N. L. Hadipour¹ · B. Kharazian^{1,4}

Received: 19 June 2020 / Accepted: 28 September 2020
© Springer-Verlag GmbH Germany, part of Springer Nature 2020

Abstract

Due to unique features in surface activity, thermal stability, electrical and thermal conductivity, and compatibility with biomolecules such as DNA and proteins, carbon-based nanoparticles are raised potential as a candidate for various applications such as catalytic processes, drug delivery, light, and electrical engineering. Based on this premise, thermodynamic features of pure, graphene, and carbon nanotube (CNT)-based gold nanoparticles (AuNPs) are investigated using molecular dynamics approach. Melting, heat capacity, thermal conductivity, contact angle of molten AuNPs, and phase transition are calculated as indicators of thermodynamic properties of pure and carbon-based AuNPs. Simulation results indicate that the presence of a carbon platform and its contact surface area has a significant role in the thermodynamic properties of AuNPs and leads the phononic heat capacity and thermal conductivity to decrease for AuNPs. The platform also causes the melting point temperature of AuNPs to increase. The melting of gold on the carbon base is of the first-order type. In addition, contact angle for molten AuNPs on the Graphene is significantly higher than the one on the CNT due to more contact area on the Graphene substrate.

Keywords Gold nanoparticles · Graphene · Nanotube · Thermodynamic properties · Molecular dynamics

Introduction

Nano-particles are one of the most promising alternatives for common metals and materials at the industrial catalytic applications due to a series of extraordinary performances such as the possibility of production in a wide range of dimensions [1], increased surface area [2], ability to chemical and physical adsorption [3], and low environmental problems compare with chemicals [4]. One of those interesting features of

nanoparticles is their catalytic activity [5]. Meanwhile, the size of nanoparticles as a catalyst has significant effects on their surface behaviors [6] and high surface-to-low volume ratio on the metallic nanoparticles such as gold, cobalt [7], and iron nanoparticles leads to make the more catalytic active sites on their surfaces causing their surface readily available to arriving reagents [8]. This unique performance in the production of catalytic active sites has promoted substantial interest and work on using the nanoparticles as one of the main candidates for a new generation of catalysts [9–12].

For instance, Balbuena et al. [13] studied the oxidation of catalytic processes on the surface (111) of Pt and Pt/PtCo/Pt₃Co using molecular dynamics. Simulation results show that the production of oxygen and water causes some changes in the structure and arrangement of catalyst top-level atoms affecting the activity and stability of the catalyst. Thermal stability is one of the key essentials of industrial catalytic structures [14], which nanoparticles as a catalyst must also have this capability. This property makes scientists look for new and more heat-stable types of catalysts. In recent years, several approaches have been proposed to increase the thermal stability of catalysts, especially nanoparticle-based catalysts [15–17] that one of these proposals is to create a base or platform for catalysts.

Electronic supplementary material The online version of this article (<https://doi.org/10.1007/s00894-020-04559-2>) contains supplementary material, which is available to authorized users.

✉ B. Kharazian
b.kharazian@modares.ac.ir

¹ Department of Physical Chemistry, Tarbiat Modares University, Tehran, Iran

² Department of Physics, Salahaddin University, Erbil, Kurdistan Region, Iraq

³ Department of Mining Engineering, Sahand University of Technology, Tabriz, Iran

⁴ Department of Pharmaceutics, Faculty of Pharmacy, Tehran University of Medical Sciences, Tehran, Iran

Table 1 Calculated lattice heat capacity for simulation systems at 300 K

System name (abbreviation)	AuNPs	AuNPs@CNT	AuNPs@Graphene
$C_{v, \text{lat}} (J \cdot \text{mol}^{-1} \cdot K^{-1})$	14.65 ± 0.01	14.35 ± 0.01	13.88 ± 0.01

For example, Sarangi et al. [18] had an investigation on the melting point temperature of silicon-based gold nanoparticle (AuNPs). Molecular dynamics simulation results show that the silicon substrate for AuNPs is found to lead a significant change on the melting point temperature of AuNPs where an AuNPs melts in lower temperatures than the one on a silicon platform. Navarro et al. [19] studied bimetallic Pt–Pd nano-alloy. In this research, the melting point temperature of pure Pt–Pd alloy was compared with the same alloy with graphite support. Their results show that the presence of graphite support causes the melting point temperature of Pt–Pd alloy to increase from 1000 to 1200 °C.

In this study, we particularly investigate the thermal characteristics of pure and carbon-based AuNPs from a molecular point of view. AuNPs, with straightforward synthesis and special physical and chemical properties such as optical, electrical, and thermal, are utilized as semiconductors and catalysts in photo-thermal therapy [20]. With a melting point above 3000 K [21] and more flexibility to adapt to host, Graphene and carbon nanotubes (CNT) are chosen as a substrate to investigate the effect of a carbon-based platform on the thermal features of AuNPs. Some investigations confirm that graphene and CNT as a substrate have a significant effect on their host's physical and physicochemical properties [22]. As a unique member of carbon-based nanoparticle family, Graphene and CNT also have a variety of extraordinary mechanical, chemical, and surface properties. Zero partial charges of carbon atoms in the Graphene structure leads to its surface to have a naturally hydrophobic behavior [23].

Similar to Graphene, CNTs are cylindrical-shaped novel nano-systems that have a wide range of applications in science, engineering, and environmental issues due to their special properties such as high mechanical strength, low weight, and flexibility [24].

Considering admissible results of simulation and modeling methods based on molecular dynamics (MD) [18, 25, 26] in the similar cases, molecular dynamics is chosen for calculating the interactions between AuNPs–Graphene and AuNPs–CNT atoms. Specifically, we study the effect of carbon base on thermal and thermodynamic properties of gold nanoparticle by using classical molecular dynamics. Thermodynamics attributes on the bare and Graphene and CNT-based AuNPs is discussed with heat capacity, thermal conductivity, and phase transition phenomena. The process of melting, the formation of molten AuNPs nano-droplet, and its contact angle on the Graphene and CNT bases are also discussed. The physicochemical and thermodynamic aspects of this investigation can be considered one of the initial steps for future fundamental studies on the development of a new generation of catalysts known as nano-catalysts.

Computational details

As shown in Fig. 1 and Table 1, three simulation systems compatible with investigation scenarios are made with PACKMOL [27] to perform the molecular dynamics studies.

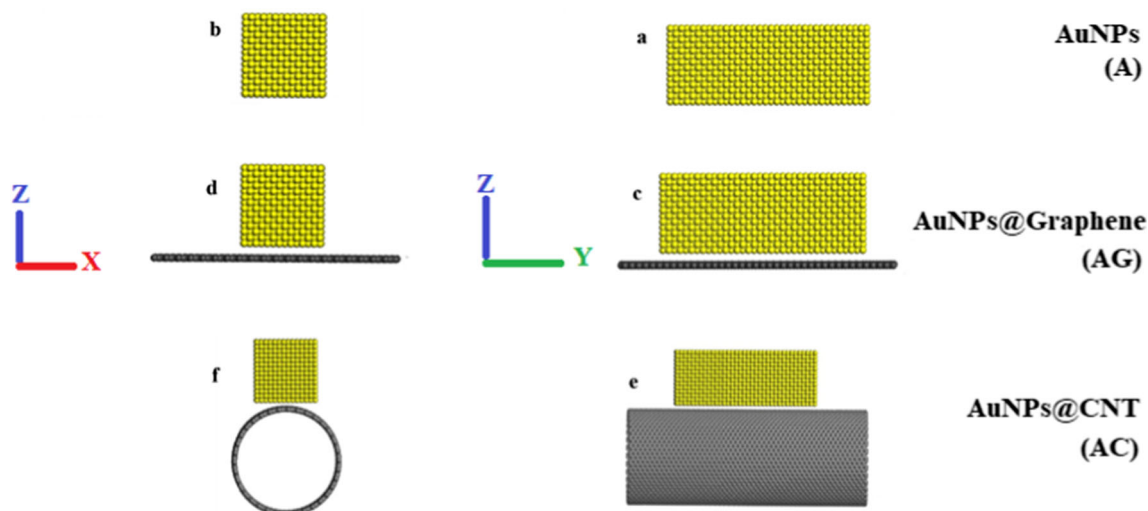
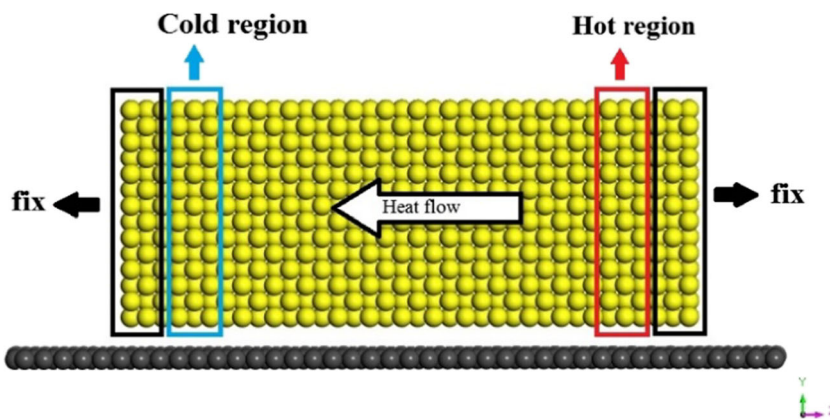


Fig. 1 Initial configuration of simulation systems, Au and C atoms are represented in yellow and black, respectively

Fig. 2 Schematics of heat flow in Graphene-based AuNPs



AuNPs simulation system (A) is performed to investigate the thermodynamics behavior of pure gold nanoparticle. To study the effect of Graphene (AuNPs@Graphene (AG)) and CNT (AuNPs@CNT (AC)) base on the thermodynamics features of AuNPs, adsorption of gold nanoparticle on the armchair configuration of Graphene and CNT surfaces and its effect on the physical and physicochemical behavior of AuNPs are simulated. The dimension of performed AuNPs in the simulation systems are $29 \times 71 \times 29 \text{ \AA}^3$ in the x -, y -, and z -directions, respectively. The shape of AuNPs was assumed to be cubic because according to Ling et al. [28], Au (111) is a mostly exposed plan in gold NP conjugates. In addition, Siming Zhang showed the most stable structure for AuNPs larger than 2 nm is the truncated-octahedral structure (fcc) [29]. The dimensions of the Graphene sheet as the substrate of AuNPs in the AG simulation system are $90 \times 90 \text{ \AA}^2$ in the x - and y -directions, respectively. The dimensions of CNT as the substrate of AuNPs in the AC simulation system are also $30 \times 90 \text{ \AA}^2$ in the x - (and z -) and y -directions, respectively. Periodic boundary conditions are considered in the x -, y -, and z -directions due to the physics of the simulation systems.

Initially, the isolated AuNPs were optimized, subsequently; Au NPs were simulated on Graphene. To evaluate the equilibrium of the considered systems, energy and entropy were measured (Fig. S1, S2). Inter- and intra-atomic interactions between nanoparticle and substrate in the simulation systems are simulated with the open-source code large-scale atomic/molecular massively parallel

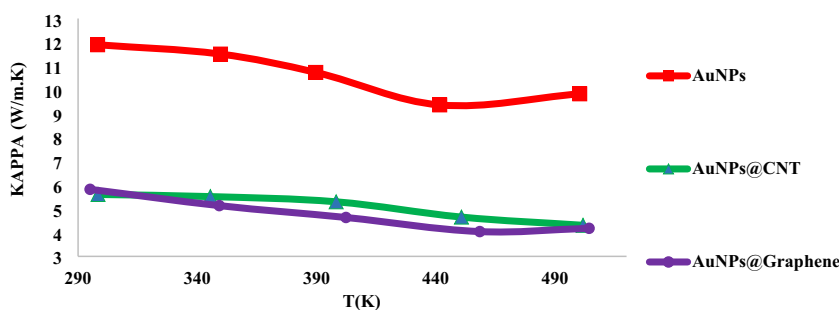
simulator (LAMMPS) [30]. Visual molecular dynamics (VMD) is used for the visualization of structures, and post-processing of simulation data [31]. The Embedded-atom method (EAM potential) is used to calculate the interactions between Au atoms [32] (Table S1). The consistent valence force field (CVFF) is used to describe bonded and non-bonded interactions between carbon and gold atoms [33, 34]. A 6–12 Lennard-Jones potential energy model [35] is used to model all non-bonded interactions. Verlet algorithm is used to integrate the motion equations for atoms in the simulation boxes. The substrate is considered fixed at its initial position during simulation time. The time-step of simulation is set to one femtosecond for all simulations. Systems are simulated for 6 ns with the constant-temperature, constant-volume ensemble (NVT), and the Nose-Hoover thermostat [36] at temperature of 300 K.

Results and discussion

Thermal conductivity

Thermal conductivity, capability of a material to transmit heat, is a thermodynamic feature of materials calculating in watts per square meter of surface area for a temperature gradient of 1-K per unit thickness of 1 m [37]. Total thermal conductivity coefficient (k_{total}) for a material is equal to the algebraic

Fig. 3 Thermal conductivity of AuNPs (red), AuNPs@CNT (green), and AuNPs@Graphene (purple)



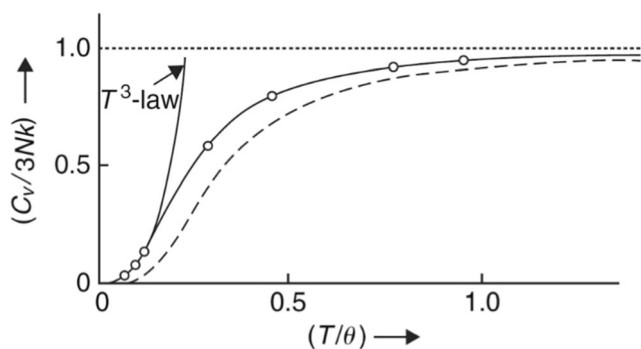


Fig. 4 Specific heat of a solid, according to the Einstein model (---) and Debye model (—)

addition of the electronic (K_{el}) and phononic (K_{phonon}) coefficient [38]. For conductive solid and metals, 90–95% of total thermal conductivity is due to electronic coefficient contribution and 5–10% of total thermal conductivity is due to phononic part contribution [39]. Based on molecular dynamics approach of this research work, the classical part of total phonon, K_{phonon} , is used to present and discuss the effect of a carbon-based platform on AuNPs thermal conductivity [40]. Figure 2 shows a schematic view of non-equilibrium molecular dynamics (NEMD) [41] simulation used to study the thermal conductivity and heat transport along Graphene-based AuNPs.

Heat flux, J , of three simulation systems are calculated by Eq. (1) where E_i is total energy, V_i is the velocity of atom i , and S_i is stress tensor. The steady state temperature gradient is created in pure and carbon-based AuNPs due to certain heat flux applying to AuNPs.

$$J = \frac{1}{V} [\sum E_i V_i - \sum S_i V_i] \tag{1}$$

Then, thermal conductivity is obtained by Eq. (2):

$$K_{phonon} = -\frac{J}{\nabla T} \tag{2}$$

where J is the flux of thermal energy or the energy transmitted across unit area per unit time, ∇T is a temperature gradient, and K_{phonon} is the thermal conductivity coefficient. The applied temperature gradient (∇T) of AuNPs on the simulations are considered from 5 to 10 K. The rage

Fig. 5 Phonon DOS of AuNPs (red), AuNPs@CNT (green), and AuNPs@Graphene (dark blue)

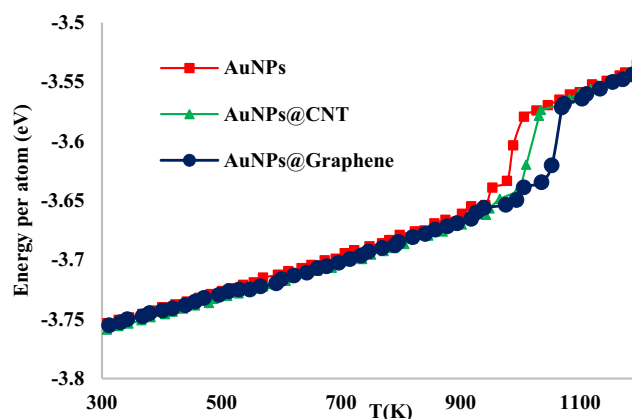
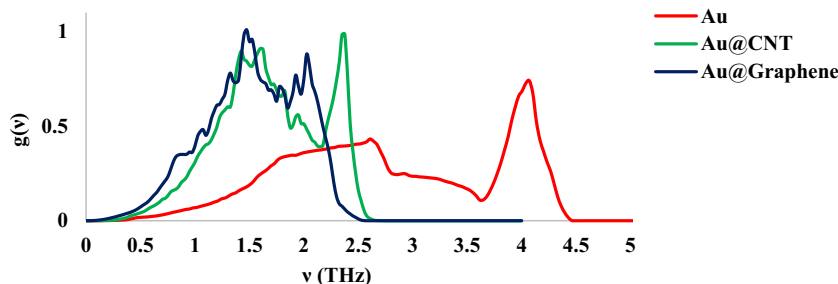


Fig. 6 Energy diagram of AuNP (red), AuNP on CNT platform (green), and AuNP on the Graphene platform (dark blue)

of temperature (ΔT) variation is considered from 300 to 500 K in the calculations. Gold total thermal conductivity is reported 317 ($\frac{w}{m.K}$) in literature [42]. In Fig. 3, thermal conductivity diagrams are shown for the simulation system. There are many common theorems about the heat capacity of solids such as the Einstein approximation theorem and the Debye approximation theorem [31]. These theorems have different behaviors in low temperatures (near to zero Kelvin) but the convergence of their volumes increases at high temperatures (Fig. 4).

In this research, the Einstein approximation theorem is used for AuNPs, AuNPs@CNT, and AuNPs@Graphene to validate the results of C_{v-lat} and K_{phonon} . Phonon density of state (DOS) is used at temperatures above 300 K to evaluate the relation between C_{v-lat} , K_{phonon} , and vibration frequency of phonon. Solid materials are considered an N harmonic oscillator by ω_0 frequency in Einstein approximation theorem. Based on this premise, total energy of solid material is given as follows:

$$U = 3N \left(\langle n \rangle + \frac{1}{2} \right) \hbar \omega_0 = 3N \frac{\hbar \omega_0}{\exp(\hbar \omega_0 / kT) - 1} + 3N \frac{\hbar \omega_0}{2} \tag{3}$$

where k is Boltzmann constant and T is temperature. Heat capacity is defined as follows:

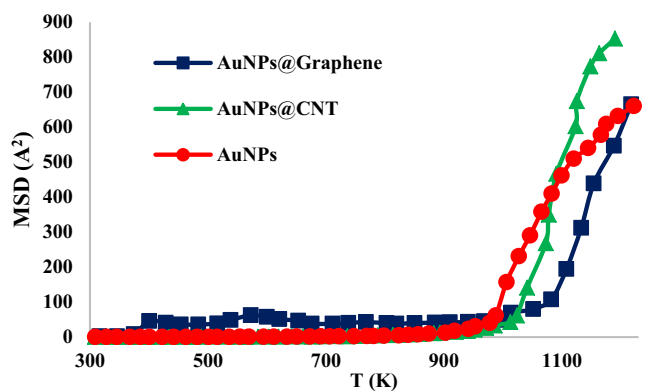


Fig. 7 MSD values for AuNPs (red), AuNPs on the CNT (green), and AuNPs on the Graphene platform (dark blue)

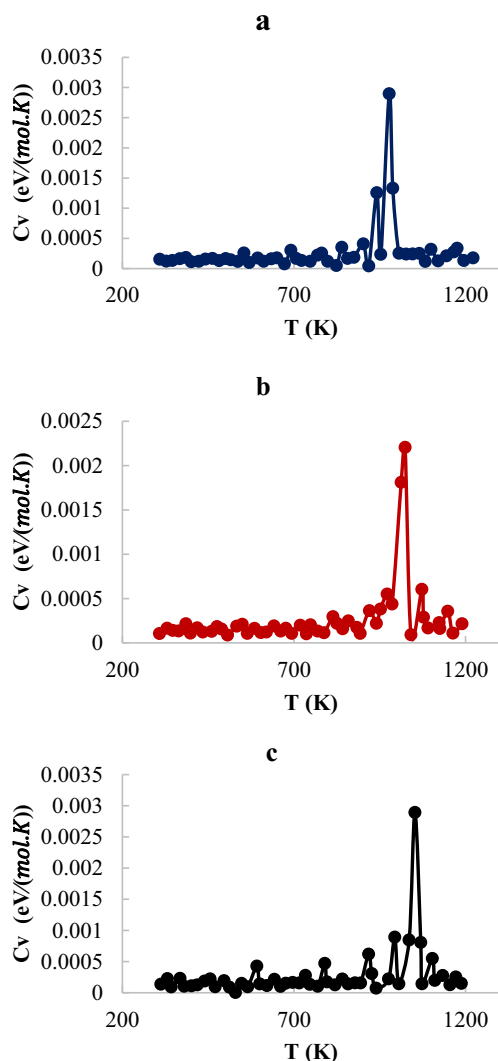


Fig. 8 Heat capacity for (a) AuNPs, (b) AuNPs on CNT, and (c) AuNPs on the Graphene platform at 300–1200 K temperature range

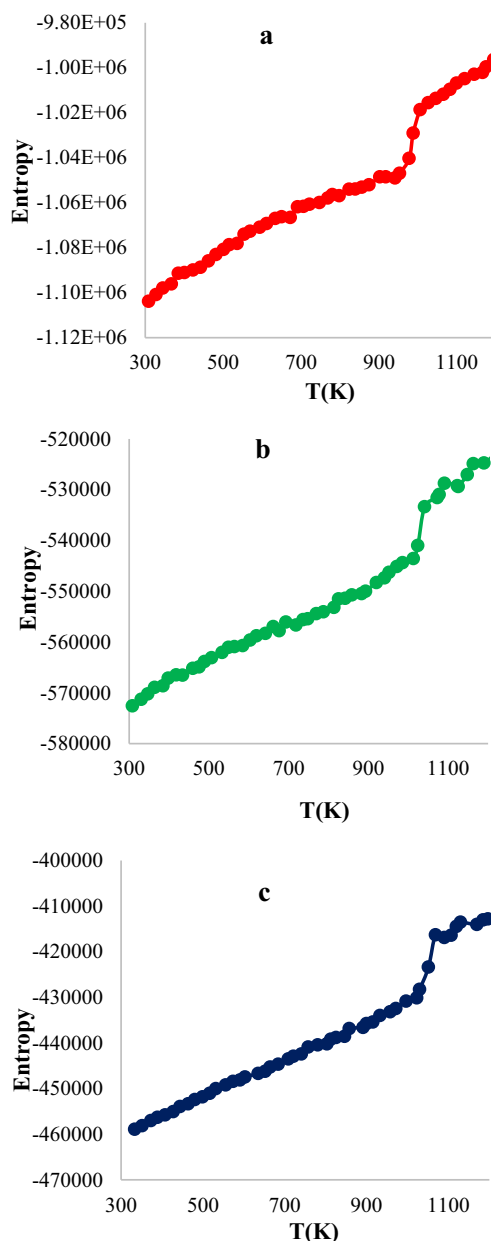


Fig. 9 Entropy for (a) AuNPs, (b) AuNPs on CNT, and (c) AuNPs on the Graphene platform at 300–1200 K temperature range

$$C_V = \left(\frac{\partial U}{\partial T} \right)_V = 3Nk \left(\frac{\hbar\omega_0}{kT} \right)^2 \frac{e^{\hbar\omega_0/kT}}{(e^{\hbar\omega_0/kT} - 1)^2} \quad (4)$$

As explained, in high temperature $\frac{\hbar\omega_0}{kT} \ll 1$ and $\exp(\hbar\omega_0/kT) \approx 1 + \frac{\hbar\omega_0}{kT}$ then C_V is obtained as follows:

$$C_V = 3Nk \left(1 + \frac{\hbar\omega_0}{kT} \right) \quad (5)$$

which shows C_V has a direct relation to ω_0 . The result of phonon DOS for three simulation systems are shown in Fig. 5. As shown in Fig. 5, pure AuNPs shows a higher phonon frequency

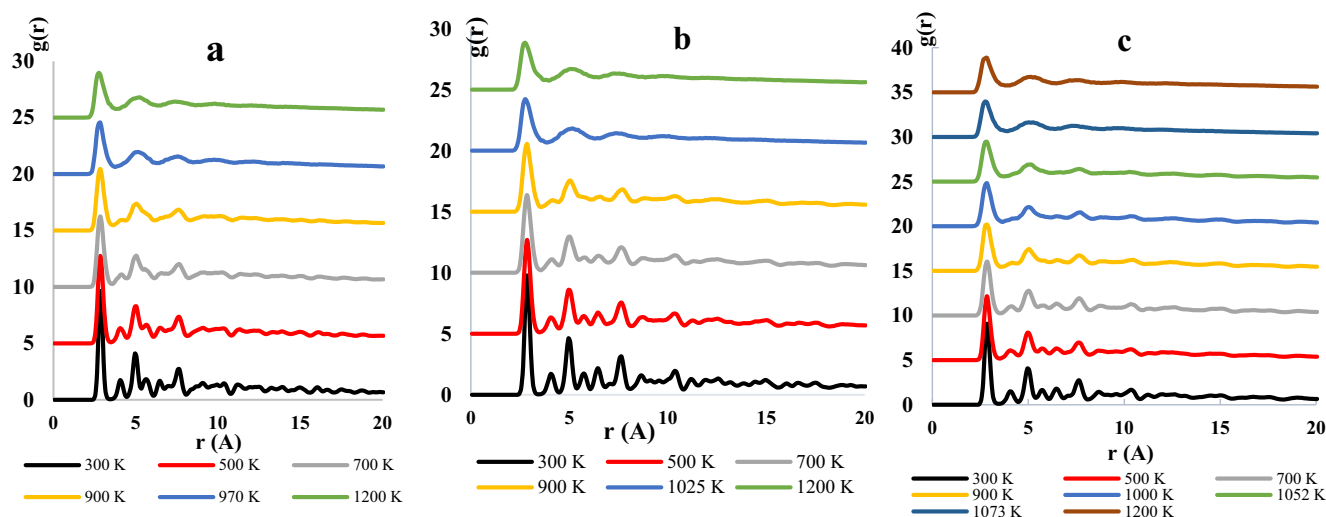


Fig. 10 RDF results for (a) AuNPs, (b) AuNPs on CNT platform, and (c) AuNPs on Graphene platform

compare with the AuNPs on the CNT and Graphene platforms. Based on the kinetic theory of gases [43] relation between thermal conductivity and heat capacity is:

$$K = \frac{1}{3}Cv\lambda \quad (6)$$

where C is heat capacity per unit volume, v is the average particle velocity, and λ is the mean free path of a particle between collisions. The thermal conductivity process of pure, CNT, and graphene-based AuNPs can be explained by Eq. (6). According to Eq. 6, there is a direct relation between K and C , and constant values for v (related to temperature) and λ (nano-cluster length) cause the trend of C and K to be the same.

The circles denote the experimental results for copper [44].

Heat capacity

Heat capacity or specific thermal is the amount of heat per unit mass of material that is required to raise the temperature by 1 °C [45]. Heat capacity at the constant volume is equal to Eq. (7) where E is total energy, K is Boltzmann constant, and T is the absolute temperature.

$$C_V = \frac{\langle E^2 \rangle - \langle E \rangle^2}{kT^2} \quad (7)$$

Table 2 Contact angle and com determination results from MD simulations

System name (abbreviation)	AuNPs@CNT	AuNPs@Graphene
Measured contact angle (°)	117	134
Center of mass (Å)	13.78 ± 0.01	15.17 ± 0.01

The calculation of lattice heat capacity for three simulated models is presented in Table 1.

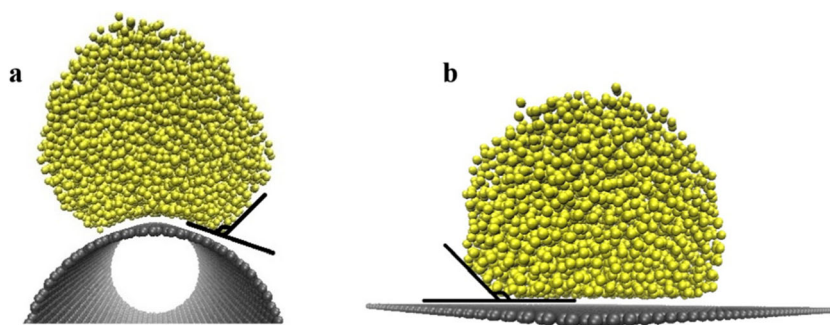
The MD-based calculation is performed at 300 K for all simulation systems. The results confirm that the carbon platform has a significant effect on lattice heat capacity because the lattice heat capacity reduces for gold nanoparticle due to the presence of carbon substrate. The results also show that heat capacity for AuNPs on the Graphene platform is lower than the one on the CNT platform confirming the effect of contact area and non-bond interactions between Gold and carbon atoms on heat capacity.

Melting point temperature

The melting point temperature of a substance is defined as the temperature at which it changes from a solid phase to a liquid phase; that is, undergoes fusion [46]. In molecular-scale studies, energy diagrams and mean square displacement (MSD) are used to analyze melting point temperature and phase change. Figure 6 shows steady values of total energy in different simulated systems where horizontal and vertical axes show temperature (K) and energy (eV) values, respectively. As seen in Fig. 6, the melting process for pure AuNP is signalized by a jump in the energy diagram at 970 K. In the carbon-based systems, AuNP on the Graphene and CNT platforms jumps in the energy diagrams are observed at 1052 K and 1025 K, respectively. The phase change from solid to liquid, melting, causes the range of motion for atoms to change from vibration movement to free movement.

In molecular systems, mean square displacement is an indicator of mobility and movement for atoms; therefore, phase change and melting point is observable by MSD

Fig. 11 Stabilized molten AuNPs nano-droplet on the (a) CNT and (b) Graphene platform



[47]. Figure 7 shows the MSD values of Au atoms as a function of temperature in different simulation systems. As seen in Fig. 7, phase transition in different simulation systems are in good agreement with energy diagrams in Fig. 6. MSD values verify that phase transition from solid to liquid for pure AuNP, CNT-based, and Graphene-based AuNP occurred at 970 K, 1025 K, and 1052 K, respectively.

Energy and MSD results show that the LJ interactions between the carbon-based platform and AuNP have a significant effect on the AuNP melting point and lead the melting point temperature of AuNP to increase. They also illustrate that melting point temperature for AuNP on the Graphene platform is higher than the one on the CNT platform due to more contact area and a further amount of LJ interactions between gold and carbon atoms.

A phase transition is a change in state from one phase (solid, liquid, or gas) to another [48]. All matters or systems in any phase and state have certain physical properties. Phase transition for a matter leads physical properties of the system like volume, viscosity, and [specific heat](#) to change. In physics and thermodynamics of materials, each system is defined by an equation of state relating state variables and describing the state of matter under a given set of physical conditions such as temperature, pressure, and volume. Equation of phase, which is a function of state, changes with phase transition. Phase transition is divided to first, second, third, fourth, and *n*-th-order categories based on the rate of derivative of the state equation. If the subcritical changes are observed in the first-order derivative of the state equation, the phase transition is first order; otherwise, the phase transition is second order (Fig. S5) [49].

Figures 8 and 9 show calculated heat capacity and entropy for pure AuNPs, AuNPs on the CNT, and the Graphene platform. The major peaks in heat capacity and entropy graphs confirm that phase transition is first order. The location of major peaks in Figs. 8 and 9 are in good agreement with previous results and prove that carbon base has a significant effect on the thermal properties of AuNPs. In addition, there are clear differences between Graphene and CNT results that confirm the more the contact area between platform and

nanoparticle, the higher the changes in the thermal property of nanoparticle.

Radial distribution function

Radial distribution function (RDF) as a known pair correlation function is a useful quantity to represent the average distribution of atoms around any given atom within molecular dynamics. RDF shows several peaks that correspond to the first, second, third, etc. coordination spheres. Fluctuation in the RDF is a strongly dependent type of matter. Solids have periodic structures, broadened peaks caused by molecules vibrating around their lattice sites, but gases do not have a regular structure. In liquid because of dynamically moving, the first coordinate sphere will occur at $\sim\sigma$, and in large r value, the distribution returns to the bulk density. RDF is a common method of structural arrangement evaluation. In Fig. 10, RDF graphs are shown for a three simulation systems in different temperatures.

In statistical mechanics, RDF is used to evaluate the density of neighboring atoms in a molecule or set of molecules or in a crystal relative to each other. RDF graph has a direct relationship with system phase and its temperature [48]. This dependency leads to a series of delta Dirac functions for a solid structure at the low temperature, while for the same structure at high temperature and liquid or gas phase, the Dirac functions convert to Gaussian distribution functions due to increase in the vibration and movement domain of atoms. RDFs are calculated relative to the gold atoms. The RDF results clearly show changes from delta Dirac function in low temperature to Gaussian distribution function in high temperature proving the melting of pure and carbon-based AuNPs. The results also confirm that the carbon platform has a significant effect on the RDF picks, and its presence causes the change from delta Dirac function to Gaussian distribution function to shift to a higher temperature which is in fair agreement with Energy and MSD results.

Contact angle of molten AuNPs

For a solid substrate in immediate contact with a liquid droplet, wetting and contact angle result from a balance of

cohesion and adhesion forces between liquid molecules and the surface atoms, respectively. Based on contact angle between the substrate and liquid droplet, solid surfaces are divided to hydrophobic and hydrophilic in behavior. On a hydrophilic surface (surface-philic), the contact angle between a liquid droplet and solid surface is lower than 90° , and liquid wets solid surface, while on a hydrophobic surface (surface-phobic), the contact angle between a liquid droplet and solid surface is higher than 90° [50].

The molten gold nano-droplets, which are used in the calculations of the contact angle, show asymmetries and a variety in values in different directions. To minimize the effect of these variations in contact angle calculations, contact angles for each nano-droplet are calculated along the z -axis in the four main sides by image processing analysis in MATLAB [23, 51], and then the mean of the measured values is considered the nano-droplet contact angle (Fig. 11 and Table 2). The position of the center of mass (COM) for the nano-droplets is also calculated along the z -axis (Table 2). As seen from Fig. 11 and Table 2, the contact angle for molten gold nano-droplet on the Graphene platform is higher than the one on the CNT platform that causes the com for nano-droplet on the Graphene to shift from 13.78 to 15.17 Å with respect to the surface. It is due to more LJ interaction between gold and carbon atoms on the Graphene platform leading to less surface energy and more surface-phobic on the Graphene platform. In general, the simulated contact angles are in good agreement with previous studies [52].

Concluding remarks

In this research work, molecular dynamics is used to perform a study on the thermodynamic features of carbon-based gold nanoparticles. Graphene and CNT are chosen as a platform to evaluate the effect of carbon base on the thermodynamic properties of AuNPs. The Graphene and CNT bases lead the melting temperature for AuNPs particles to increase from 970 K to 1052 K and 1025 K, respectively, showing the melting temperature of AuNPs on the CNT substrate is lower than the one on the Graphene. The effect of the platform on the phononic heat capacity ($C_{v,lat}$) and thermal conductivity (K_{phonon}) of AuNPs is also significant and reduces them. On the carbon bases, a clear difference in the surface tension for molten AuNPs is observed leading the contact angle for molten AuNPs on the Graphene to be significantly higher than the one on the CNT. In sum, outcomes reveal that the carbon platform and its contact surface area have a direct effect on the physical and physicochemical properties of AuNPs. In General, the results are in good agreement with previous studies and show that carbon-based nanoparticles can be considered a promising alternative to various common laboratory

and industrial-scale catalytic applications due to its higher thermal stability.

Funding MD simulations and post-simulation analysis were performed using computing clusters at the Tarbiat Modares University, Tehran, Iran.

References

1. Fedlheim DL, Foss CA (2001) Metal nanoparticles: synthesis, characterization, and applications. CRC press
2. Goncalves G, Marques PA, Granadeiro CM, Nogueira HI, Singh M, Gracio J (2009) Surface modification of graphene nanosheets with gold nanoparticles: the role of oxygen moieties at graphene surface on gold nucleation and growth. *Chem Mater* 21:4796–4802
3. Bhattacharya P, Lin S, Turner JP, Ke PC (2010) Physical adsorption of charged plastic nanoparticles affects algal photosynthesis. *J Phys Chem C* 114:16556–16561
4. Yang S, Pelton R, Raegen A, Montgomery M, Dalnoki-Veress K (2011) Nanoparticle flotation collectors: mechanisms behind a new technology. *Langmuir* 27:10438–10446
5. Hvolbæk B, Janssens TV, Clausen BS, Falsig H, Christensen CH, Nørskov JK (2007) Catalytic activity of au nanoparticles. *Nano Today* 2:14–18
6. Sun L, Yang X, Wu B, Tang L (2011) Molecular simulation of interaction between passivated gold nanoparticles in supercritical CO₂. *J Chem Phys* 135:204703
7. Dou S, Li X, Tao L, Huo J, Wang S (2016) Cobalt nanoparticle-embedded carbon nanotube/porous carbon hybrid derived from MOF-encapsulated co₃O₄ for oxygen electrocatalysis. *Chem Commun* 52:9727–9730
8. Sanchez A, Abbet S, Heiz U, Schneider W-D, Häkkinen H, Barnett R, Landman U (1999) When gold is not noble: nanoscale gold catalysts. *J Phys Chem A* 103:9573–9578
9. Krauss TD, Eisenberg R, Holland P, Qiu F, Han Z (2019) Methods for producing hydrogen using nanoparticle-catalyst mixtures. Google Patents
10. Tafrihi H, Sadeghzadeh S, Molaei F, Siavoshi H (2020) Investigating the effects of adding hybrid nanoparticles, graphene and boron nitride nanosheets, to octadecane on its thermal properties. *RSC Adv* 10:14785–14793
11. Elsayed I, Mashaly M, Eltaweel F, Jackson MA (2018) Dehydration of glucose to 5-hydroxymethylfurfural by a core-shell Fe₃O₄@ SiO₂-SO₃H magnetic nanoparticle catalyst. *Fuel* 221:407–416
12. Schlexer P, Widmann D, Behm RJR, Pacchioni G (2018) CO oxidation on a Au/TiO₂ nanoparticle catalyst via the au-assisted Mars–van Krevelen Mechanism. *ACS Catal* 8:6513–6525
13. Callejas-Tovar R, Liao W, Martinez de la Hoz JM, Balbuena PB (2011) Molecular dynamics simulations of surface oxidation on Pt (111) and Pt/PtCo/Pt₃Co (111). *J Phys Chem C* 115:4104–4113
14. Puértolas B, Mayoral Á, Arenal R, Solsona B, Moragues A, Murcia-Mascaros S, Amorós P, Hungria AB, Taylor SH, García T (2015) High-temperature stable gold nanoparticle catalysts for application under severe conditions: the role of TiO₂ nanodomains in structure and activity. *ACS Catal* 5:1078–1086
15. Shang Z, Li S, Li L, Liu G, Liang X (2017) Highly active and stable alumina supported nickel nanoparticle catalysts for dry reforming of methane. *Appl Catal B Environ* 201:302–309

16. Arrigo R, Schuster ME, Xie Z, Yi Y, Wowsnick G, Sun LL, Hermann KE, Friedrich M, Kast P, Hävecker M (2015) Nature of the N–Pd interaction in nitrogen-doped carbon nanotube catalysts. *ACS Catal* 5:2740–2753
17. Onn TM, Zhang S, Arroyo-Ramirez L, Chung Y-C, Graham GW, Pan X, Gorte RJ (2015) Improved thermal stability and methane-oxidation activity of Pd/Al₂O₃ catalysts by atomic layer deposition of ZrO₂. *ACS Catal* 5:5696–5701
18. Sarangi S, Satyam P, Nayak S, Mahanti S (2017) Molecular dynamics simulation studies of gold nano-cluster on silicon (001) surface. *Indian J Phys* 91:853–859
19. Fernández Navarro CJ, Mejía Rosales S (2013) Molecular dynamics of free and graphite-supported Pt-Pd nanoparticles. *Adv Nanoparticles* 2:323–328
20. Huang X, El-Sayed MA (2010) Gold nanoparticles: optical properties and implementations in cancer diagnosis and photothermal therapy. *J Adv Res* 1:13–28
21. Ganz E, Ganz AB, Yang L-M, Dornfeld M (2017) The initial stages of melting of graphene between 4000 K and 6000 K. *Phys Chem Chem Phys* 19:3756–3762
22. Mittal G, Dhand V, Rhee KY, Park S-J, Lee WR (2015) A review on carbon nanotubes and graphene as fillers in reinforced polymer nanocomposites. *J Ind Eng Chem* 21:11–25
23. Mabudi A, Noaparast M, Gharabaghi M, Vasquez V (2019) A molecular dynamics study on the wettability of graphene-based silicon dioxide (glass) surface. *Colloids Surf A Physicochem Eng Asp* 569:43–51
24. Filleter T, Bernal R, Li S, Espinosa HD (2011) Ultrahigh strength and stiffness in cross-linked hierarchical carbon nanotube bundles. *Adv Mater* 23:2855–2860
25. Font F, Bresme F (2018) Transient melting at the nanoscale: a continuum heat transfer and nonequilibrium molecular dynamics approach. *J Phys Chem C* 122:17481–17489
26. Vo TQ, Kim BH (2017) Molecular dynamics study of thermodynamic properties of nanoclusters for additive manufacturing. *Int J Precis Eng Manuf Green Technol* 4:301–306
27. Martínez L, Andrade R, Birgin EG, Martínez JM (2009) PACKMOL: a package for building initial configurations for molecular dynamics simulations. *J Comput Chem* 30:2157–2164
28. Pedireddy S, Lee HK, Tjiu WW, Phang IY, Tan HR, Chua SQ, Troadec C, Ling XY (2014) One-step synthesis of zero-dimensional hollow nanoporous gold nanoparticles with enhanced methanol electrooxidation performance. *Nat Commun* 5:4947
29. Zhang S (2011) Molecular dynamics simulation of gold nanoparticles and surface stress effect. Lehigh University
30. Plimpton S (1995) Fast parallel algorithms for short-range molecular dynamics. *J Comput Phys* 117:1–19
31. Humphrey W, Dalke A, Schulten K (1996) VMD: visual molecular dynamics. *J Mol Graph* 14:33–38
32. Daw MS, Foiles SM, Baskes MI (1993) The embedded-atom method: a review of theory and applications. *Mater Sci Rep* 9:251–310
33. Dauber-Osguthorpe P, Roberts VA, Osguthorpe DJ, Wolff J, Genest M, Hagler AT (1988) Structure and energetics of ligand binding to proteins: Escherichia coli dihydrofolate reductase-trimethoprim, a drug-receptor system. *Proteins Struct Funct Bioinf* 4:31–47
34. Yuan Q, Zhu X, Lin K, Zhao Y-P (2015) Molecular dynamics simulations of the enhanced recovery of confined methane with carbon dioxide. *Phys Chem Chem Phys* 17:31887–31893
35. Lennard-Jones JE (1931) Cohesion. *Proc Phys Soc* 43:461
36. Hoover WG (1985) Canonical dynamics: equilibrium phase-space distributions. *Phys Rev A* 31:1695
37. Holman JP (1986) Heat transfer. McGraw-hill, New York
38. Rastogi A, Rajpoot P, Rastogi R, Verma UP (2019) Ab-initio study of electronic, optical, thermal, and transport properties of Cr₄AlB₆. *Int J Quantum Chem* 119:e25897
39. Jain A, McGaughey AJ (2016) Thermal transport by phonons and electrons in aluminum, silver, and gold from first principles. *Phys Rev B* 93:081206
40. Ahadi Z, Shadman Lakmehsari M, Kumar Singh S, Davoodi J (2017) Stability and thermal behavior of molybdenum disulfide nanotubes: nonequilibrium molecular dynamics simulation using REBO potential. *J Appl Phys* 122:224303
41. Mohebbi A (2012) Prediction of specific heat and thermal conductivity of nanofluids by a combined equilibrium and non-equilibrium molecular dynamics simulation. *J Mol Liq* 175:51–58
42. Chen G, Hui P (1999) Thermal conductivities of evaporated gold films on silicon and glass. *Appl Phys Lett* 74:2942–2944
43. Dunne TG (1987) Physical chemistry, (Levine, Ira N.). ACS Publications
44. Pathria R, Beale PD (2011) Statistical mechanics. Elsevier, New York
45. Shrivastava A (2018) Introduction to plastics engineering. William Andrew
46. Stauffer E, Dolan JA, Newman R (2007) Fire debris analysis. Academic Press
47. Soma T, Kagaya HM, Nishigaki M (1983) Mean-square displacement and Lindeman's criterion for melting of alkali metals. *Phys Status Solidi B* 115:273–276
48. Fegley Jr B (2012) Practical chemical thermodynamics for geoscientists. Academic Press
49. Atkins PW, De Paula J, Keeler J (2018) Atkins' physical chemistry. Oxford University Press
50. Hubbe MA, Koukoulas AA (2016) Wet-laid nonwovens manufacture—chemical approaches using synthetic and cellulosic fibers. *BioResources* 11:5500–5552
51. Mabudi A, Noaparast M, Gharabaghi M, Vasquez V (2019) Polystyrene nanoparticles as a flotation collector: a molecular dynamics study. *J Mol Liq* 275:554–566
52. Davoodi J, Safaralizade M, Yarifard M (2016) Molecular dynamics simulation of a gold nanodroplet in contact with graphene. *Mater Lett* 178:205–207

Publisher's note Springer Nature remains neutral with regard to jurisdictional claims in published maps and institutional affiliations.